Fast directional hard x-ray diagnostic for high-frequency energetic-electron fluctuations in the QUEST spherical tokamak

Ikezoe, Ryuya
Research Institute for Applied Mechanics(RIAM), Kyushu University

Shirai, Y
Interdisciplinary Graduate School of Engineering Sciences(IGSES), Kyushu University

Kawase, S
Interdisciplinary Graduate School of Engineering Sciences(IGSES), Kyushu University

Onchi, T
Research Institute for Applied Mechanics(RIAM), Kyushu University

他

出版情報：Review of Scientific Instruments. 97 (9), 2026-09-23. AIP Publishing
バージョン：

Fast directional hard X-ray diagnostic for high-frequency energetic-electron fluctuations in the QUEST spherical tokamak

R. Ikezoe,[1, a)] Y. Shirai,[2] S. Kawase,[2] T. Onchi,[1] K. Hanada,[1] M. Hasegawa,[1] H. Idei,[1] T. Ido,[1] T. Kinoshita,[1] Y. Nagashima,[1] T. Kawate,[3] and L.F. Delgado-Aparicio[4]
[1)] *RIAM, Kyushu University, Fukuoka 816-8580, Japan*
[2)] *IGSES, Kyushu University, Fukuoka 816-8580, Japan*
[3)] *National Institutes for Quantum Science and Technology, Ibaraki 311-0193, Japan*
[4)] *Princeton Plasma Physics Laboratory, NJ 08540, USA*

(Dated: 5 August 2026)

A fast directional hard X-ray (HXR) diagnostic system has been developed for the QUEST spherical tokamak using plastic scintillators coupled to photomultiplier tubes. During intense HXR emission, the detector response transitioned from pulse-counting to current-mode operation, enabling observation of high-frequency fluctuations in the HXR signal. A clear correspondence was observed between HXR and magnetic fluctuations, while directional differences were identified among forward-, backward-, and vertical-viewing configurations. The developed technique establishes high-frequency HXR fluctuation measurements as a new diagnostic of energetic-electron dynamics, opening a new experimental window into wave–particle interactions through direct measurements of energetic-electron fluctuations.

I. INTRODUCTION

High-frequency modes driven by runaway or energetic electrons are widely observed in magnetically confined plasmas[1–3] and are expected to play an important role in the mitigation of runaway electron (RE) beams during disruptions.[4,5] In particular, a pronounced correlation between the plasma current decay rate and mode amplitude has been reported,[6] indicating strong coupling between energetic-electron-driven modes and global plasma behavior. However, the direct connection between these modes and the underlying dynamics of energetic electrons remains largely unresolved.

Recently, high-frequency fluctuations in hard X-ray (HXR) emission have been identified,[7] providing a new experimental basis for directly probing energetic-electron dynamics. Since HXR emission originates from bremsstrahlung radiation produced by energetic electrons, fluctuations in HXR intensity reflect the behavior of the emitting electron population and provide access to collective oscillatory dynamics associated with wave–particle interactions.

HXR diagnostics have long been employed in magnetic-confinement fusion devices to investigate energetic and runaway electrons through bremsstrahlung emission.[8,9] Many HXR diagnostics have relied on pulse-counting spectrometers to measure HXR energy spectra and their temporal evolution. Various detector technologies have been employed for this purpose, each optimized for different experimental requirements. Among the available detector technologies, scintillation detectors remain one of the most widely used detector technologies for HXR diagnostics because of their fast response. Considerable efforts have therefore been devoted to improving their count-rate capability while maintaining adequate energy resolution. For example, BGO scintillators have been successfully employed for runaway-electron diagnostics,[10] while YAP:Ce scintillators, with a decay time of approximately 25 ns,[11] and $LaBr_3$(Ce) scintillators, with an even shorter decay time of approximately 16 ns,[12] have enabled progressively higher count-rate HXR measurements. More recently, advanced HXR diagnostics incorporating multi-chord and imaging capabilities, together with reconstruction techniques, have enabled spatially resolved measurements and reconstruction of runaway-electron distributions, providing new insights into runaway-electron physics.[13–17] These advancements have established HXR diagnostics as an important diagnostic tool for runaway-electron studies in fusion plasmas. However, detector selection generally involves a trade-off between energy resolution and temporal response. To the best of our knowledge, no HXR diagnostic has previously been optimized specifically for resolving HXR fluctuations in the tens-to-hundreds-of-megahertz range.

To address this limitation, a directional HXR diagnostic system has been developed that combines nanosecond-scale temporal response with directional sensitivity. The system employs a pair of plastic scintillator detectors, with a scintillation decay time of approximately 1.4 ns, coupled to photomultiplier tubes (PMTs) and arranged in a dual-viewing geometry to distinguish forward and backward bremsstrahlung emission relative to the direction of electron motion. Although plastic scintillators provide poorer energy resolution than inorganic scintillators and semiconductor detectors, their ultrafast scintillation response makes them particularly suitable for resolving high-frequency HXR fluctuations. Simultaneous pulse-height spectroscopy and high-bandwidth waveform acquisition enable both conventional HXR measurements and directional observations of high-frequency HXR fluc-

a)ikezoe@triam.kyushu-u.ac.jp

tuations up to the hundreds-of-megahertz range.

In this paper, the design, characterization, and initial application of the developed diagnostic system are presented using plasmas in the Q-shu University Experiment with Steady-State Spherical Tokamak (QUEST).[18,19] The temporal response and directional measurement capability of the system are demonstrated through observations of HXR fluctuations. The developed diagnostic provides a new experimental capability for investigating energetic-electron dynamics and their coupling to energetic-electron-driven modes.

II. FAST HARD X-RAY DIAGNOSTIC SYSTEM

To resolve high-frequency HXR fluctuations associated with energetic-electron dynamics, a diagnostic system was developed with particular emphasis on fast temporal response. Since the targeted fluctuations extend into the tens-to-hundreds-of-MHz range, a sufficiently high detected X-ray flux is required to maintain statistical reliability on these time scales. To achieve this, the detector system was designed to be compact and installable in close proximity to the plasma, thereby maximizing the detected X-ray flux.

The system consists of two identical detector units that can be deployed at different viewing locations, enabling simultaneous measurements along multiple lines of sight for directional fluctuation studies.

A. Detector Design

The detector sensor consists of an EJ-228 plastic scintillator optically coupled to a Hamamatsu H3164-10 photomultiplier tube (PMT) assembly, as shown in Fig. 1. EJ-228 is a fast plastic scintillator with a decay time of approximately 1.4 ns and an emission peak wavelength of approximately 391 nm. The H3164-10 PMT assembly was operated at a bias voltage of −1.1 kV throughout the experiments. When hard X-rays interact with the scintillator, scintillation photons are generated in the EJ-228 and subsequently converted into electrical pulses by the PMT. Owing to the sub-nanosecond response of the PMT, the overall temporal response of the detector is primarily determined by the scintillation decay characteristics of the EJ-228 together with the parasitic capacitance of the signal transmission and readout circuitry.

The scintillator was fabricated in a cylindrical shape with a diameter of 8 mm and a thickness of 15 mm, matching the 8-mm effective photocathode diameter of the PMT. Optical coupling grease was applied between the scintillator and PMT window to maximize light collection efficiency. To further enhance light collection, the scintillator was wrapped with three layers of 150-nm-thick aluminized Mylar film serving as a reflective layer. The assembly was subsequently covered with a

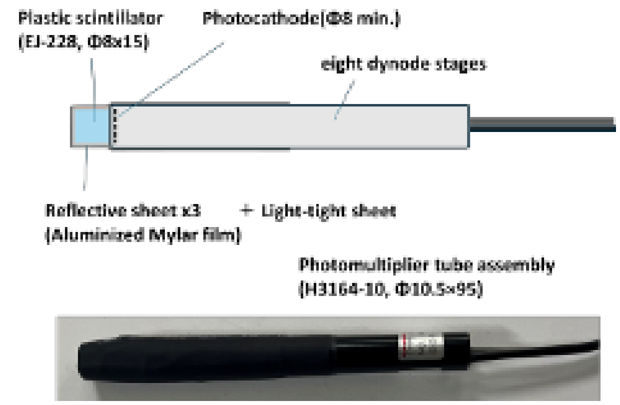

FIG. 1. Schematic diagram of the hard X-ray detector composed of an EJ-228 plastic scintillator coupled to a photomultiplier tube (PMT).

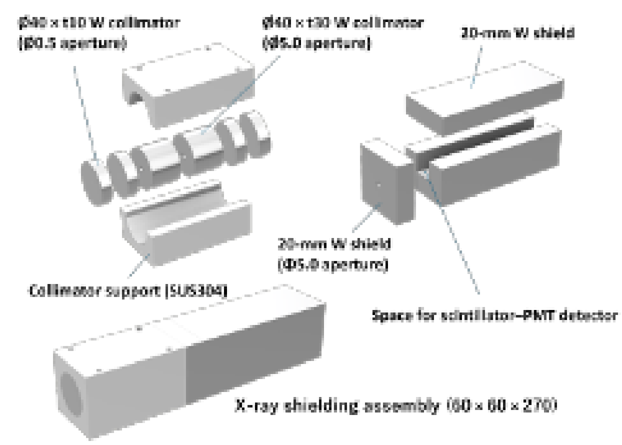

FIG. 2. Schematic diagram of the X-ray shielding and collimation assembly used for the hard X-ray detector.

light-tight sheet to suppress ambient light intrusion and ensure stable detector operation.

A schematic diagram of the collimator and X-ray shielding assembly is shown in Fig. 2, where the scintillator–PMT detector described in Fig. 1 is installed in the designated detector space. The detector is surrounded by a dedicated X-ray shielding structure designed to suppress off-axis and scattered X-rays, thereby ensuring that the measured signal is dominated by radiation entering through the collimator aperture.

The primary X-ray shielding block consists of a 20-mm-thick tungsten structure, providing substantial attenuation of hard X-rays. The 20-mm-thick tungsten shielding provides essentially complete attenuation of 100-keV X-rays and effectively suppresses higher-energy photons, reducing the transmission to approximately 1% at 500 keV and 7% at 1 MeV. Since the majority of HXR emissions observed in QUEST are below 500 keV, this shielding performance is sufficient to effectively suppress off-axis radiation. In addition, the entire shielding assembly is enclosed within a 15-mm-thick iron housing. The assembly is positioned and fixed on a horizontal support stage. The iron housing provides additional attenuation of scattered radiation as well as magnetic shielding for the PMT. Furthermore, because the detector is oriented such that the collimator points toward the plasma, most background X-rays enter the shielding structure at oblique angles. As a result, the effective path length through the shielding material is significantly greater than the nominal thickness, further improving the shielding performance.

The collimator assembly consists of four tungsten plates with a diameter of 40 mm and a thickness of 10 mm, each equipped with a 0.5-mm-diameter aperture, together with two 30-mm-thick tungsten plates containing 5.0-mm-diameter apertures. By changing the number and arrangement of these collimator elements, the effective viewing angle can be adjusted according to the experimental requirements. For the typical configuration used in this study, two 0.5-mm-diameter apertures separated by 100 mm define an effective full viewing angle of approximately 0.57°, corresponding to a field-of-view diameter of approximately 15 mm at a distance of 1.5 m from the collimator. This configuration provides sufficient spatial resolution while allowing the detector to be positioned close to the plasma to maximize the detected X-ray flux, thereby enabling investigation of the spatial structure of HXR fluctuations.

B. Detector Installation on QUEST

Two identical fast hard X-ray detectors, denoted FHX1 and FHX2, were installed on QUEST as shown in Fig. 3. The detectors had tangency radii of approximately 0.4 m and viewed regions located approximately 0.2 m outside the center stack ($R \simeq 0.22$ m). The plasma was initiated using second-harmonic electron cyclotron (EC) startup with 28-GHz microwave injection at a power of approximately 150 kW.[20,21] The resulting plasma current flowed clockwise when viewed from above. Energetic electrons accelerated during EC startup predominantly traveled in the counterclockwise toroidal direction and are considered to carry the dominant fraction of the plasma current, whereas current components associated with the thermal plasma, such as the bootstrap current, are expected to be much smaller because of the relatively low plasma pressure.

FHX2 was fixed in the forward-viewing configuration to observe bremsstrahlung emission in the forward direction relative to the dominant energetic-electron motion. In the present study, FHX1 was operated in three viewing configurations—backward-viewing, vertical-viewing, and forward-viewing—to investigate the directional dependence of HXR fluctuations. Comparison among these configurations provides information on the directional properties of the energetic-electron population contributing to the measured HXR signals.

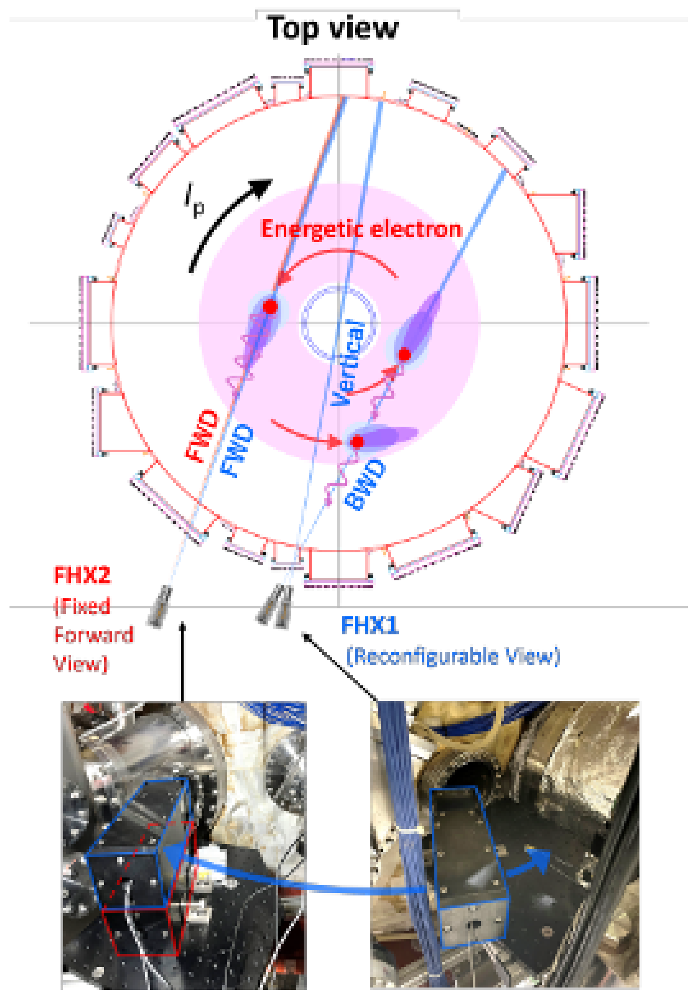

FIG. 3. Overview of the fast hard X-ray (FHX) diagnostic system installed on QUEST, including detector locations, viewing geometries, detector photographs, and a schematic illustration of the bremsstrahlung angular distribution. FHX2 was fixed in the forward-viewing configuration, whereas FHX1 was reconfigured between backward-, vertical-, and forward-viewing configurations.

The diagnostic concept relies on the energy dependence of the bremsstrahlung angular distribution. Bremsstrahlung emitted by electrons with energies above approximately 100 keV is strongly concentrated in the forward direction, whereas emission from lower-energy electrons is distributed over a much broader angular range. Because the diagnostic measures line-integrated radiation and the magnetic field lines are curved, radiation originating from the low-field side can contribute to all viewing configurations, particularly for lower-energy electrons with broad bremsstrahlung angular distributions. Accordingly, directional differences observed in the HXR signals are expected to be predominantly associated with the high-energy electron population.

C. Data Acquisition and Signal Processing

The output signal from each PMT was divided using a 50-Ω two-way resistive power divider (PE2084, Pasternack) and simultaneously routed to a digital pulse processor (DPP) and a high-speed oscilloscope. This configuration enabled simultaneous pulse-height analysis and HXR fluctuation measurements. Pulse-height spectra were acquired using a DPP (APV8104-14, TechnoAP) equipped with a 1-GHz digital processing clock. The high processing speed is well suited for the nanosecond-scale pulses generated by the fast scintillator–PMT detector. An approximate pulse-height calibration was established from Compton-edge measurements using standard gamma-ray sources. For fluctuation measurements, the PMT signals were digitized using a high-speed oscilloscope (HDO8038A, Teledyne LeCroy) with a bandwidth of 350 MHz. The signals were transmitted from the PMTs to the data-acquisition system through identical 10-m-long 50-Ω RG-223/U coaxial cables. According to the manufacturer's specifications, the attenuation over the cable length is approximately 2 dB within the frequency range of interest. A 225-MHz low-pass filter (PE8722, Pasternack) was inserted before the oscilloscope input to provide analog anti-aliasing filtering prior to digitization. The signals were sampled at 500 MS/s, corresponding to a Nyquist frequency of 250 MHz. Waveforms were recorded using a memory depth of 250 Mpoints per channel, enabling continuous acquisition over approximately 0.5 s.

III. DETECTOR CHARACTERIZATION AND INITIAL RESULTS

A. Transition from Pulse-Counting to Current Mode

Figure 4 compares the temporal evolution of the DPP count rate, R_{DPP}, with the plasma current, I_{p}, and the PMT output signal, V_{PMT}. Enlarged views of the PMT waveform are presented in Figs. 4(c)–4(f), together with the signal from a magnetic pickup coil installed on the center stack inside the vacuum vessel.

The HXR count rate began to increase noticeably once the plasma current exceeded approximately 20 kA and continued to rise during the EC current-drive (ECCD) phase, indicating enhanced production of energetic electrons. Following termination of the EC power injection, the count rate decreased substantially, although detectable HXR emission remained throughout the discharge. During the subsequent plasma-current decay phase, intermittent bursts of HXR emission were observed, each accompanied by a rapid decrease in I_{p}. Such bursts are commonly observed in QUEST and are attributed to transient interactions between the plasma and plasma-facing components, resulting in enhanced thick-target bremsstrahlung emission.

At approximately $t \sim 3.34$ s, a major loss of plasma

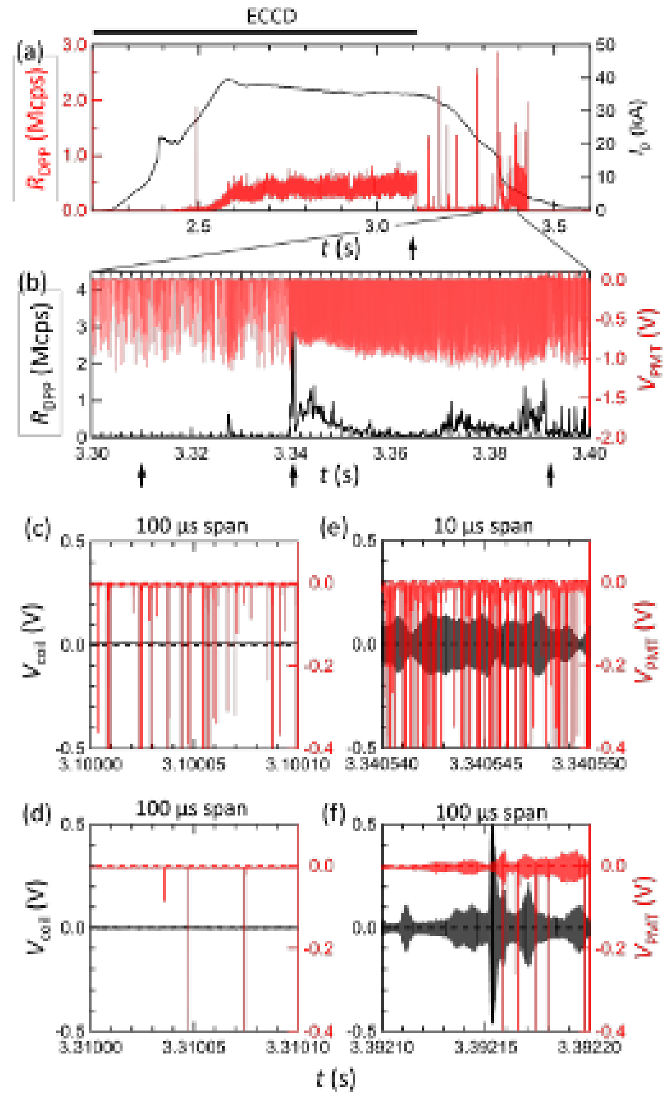

FIG. 4. Temporal evolution of R_{DPP}, I_{p}, and V_{PMT} for Shot #57062. Panels (c)–(f) present enlarged views of the PMT waveform together with the corresponding magnetic pickup coil signal.

equilibrium triggered a rapid plasma-current collapse. The resulting toroidal electric field accelerated energetic electrons and enhanced the velocity-space anisotropy, leading to the excitation of intense high-frequency magnetic fluctuations, as evidenced by the magnetic pickup-coil signal shown in Figs. 4(e) and 4(f).

When the HXR intensity was sufficiently low, individual voltage pulses were clearly resolved in the PMT waveform, as shown in Figs. 4(c) and 4(d). In this regime, the detector operated in a conventional pulse-counting mode, where both pulse height and count rate provided meaningful information on the incident radiation.

During the rapid plasma-current decay phase, the DPP count rate ceased to provide a reliable measure of the HXR intensity. Inspection of the raw PMT waveform revealed a gradual transition from isolated pulses to a densely overlapping signal with an oscillatory component. In this regime, pulse pile-up prevents reliable event identification by the DPP algorithm, rendering the count rate an inadequate indicator of the actual photon flux.

The waveform in Fig. 4(e) represents an intermediate state between pulse-counting and current-mode operation, where pulse pile-up and baseline distortion become significant. In contrast, Fig. 4(f) exhibits a continuous oscillatory waveform characteristic of current-mode detection, in which individual HXR events are no longer resolved and the detector output reflects fluctuations in the average scintillation intensity.

A notable feature of the current-mode signal is its temporal correspondence with the simultaneously measured magnetic-coil signal. Since the two diagnostics measure different physical quantities—electromagnetic fluctuations and energetic-electron-induced HXR emission, respectively—this correspondence suggests a direct coupling between wave activity and energetic-electron dynamics. The observed bipolar waveform does not imply negative X-ray intensity, but instead reflects the AC-coupled response of the detection system to fluctuations around the mean anode current. Pulse pile-up, together with possible gain compression caused by space-charge effects at high instantaneous signal levels, may further contribute to the transition from pulse-counting to current-mode behavior.

These observations indicate a transition from pulse-counting to current-mode operation during intense HXR emission, enabling direct observation of fast HXR fluctuations associated with energetic-electron dynamics.

B. HXR fluctuation measurement in QUEST

Figure 5 shows the temporal evolution of the normalized fluctuation spectrum during the plasma-current decay phase. To facilitate comparison among different diagnostics, the fluctuation spectra were normalized by the square of the local RMS envelope of each signal, $P_{\mathrm{N}}(f,t) = \frac{PSD(f,t)}{S_{\mathrm{env}}(t)^2}$, where $S_{\mathrm{env}}(t)$ denotes the moving RMS envelope of the corresponding waveform. This normalization suppresses variations in the absolute signal level and highlights the relative fluctuation activity.

Strong magnetic fluctuations are observed over a broad frequency range extending to approximately 200 MHz. At frequencies below approximately 80 MHz, similar spectral structures are observed in both the magnetic and HXR signals, although their detailed evolution differs. In particular, fluctuation components near 70–75 MHz exhibit relatively stronger signatures in the HXR spectra, and noticeable differences between the forward- and backward-viewing detectors are observed, especially in the 65–70 MHz range. These observations suggest that HXR fluctuations provide access to aspects of energetic-electron dynamics, including directional properties, that

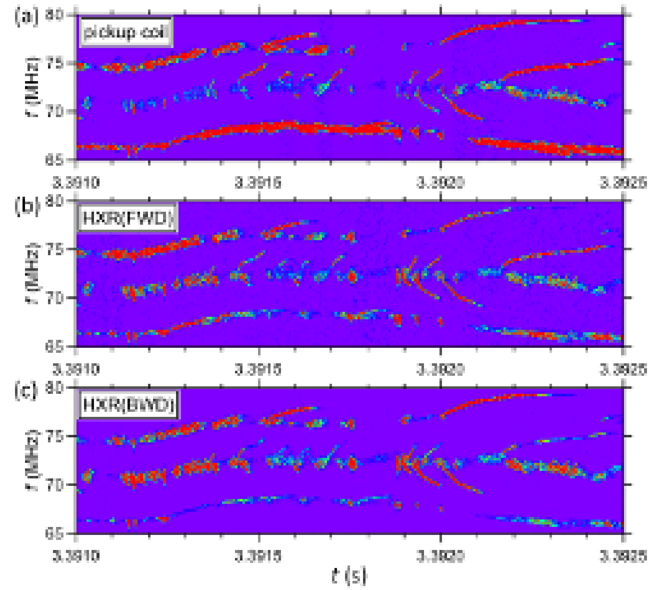

FIG. 5. Time evolution of the normalized fluctuation spectrum, $P_{\mathrm{N}}(f)$, for Shot #57068. Panels (a), (b), and (c) correspond to the magnetic pickup coil, FWD HXR, and BWD HXR signals, respectively.

are not directly reflected in the magnetic fluctuation amplitude.

To assess directional sensitivity and distinguish viewing-geometry effects from detector-dependent variations, the normalized fluctuation spectra were integrated over a 10-ms interval (3.39–3.40 s) during the period of strongest mode activity associated with the rapid plasma-current decay, as shown in Fig. 6. For the discharge shown in Fig. 6(a), this interval fully encompasses the expanded time window presented in Fig. 5 (3.3910–3.3925 s). In all cases, the magnetic spectra exhibit broad-band activity extending above 100 MHz, whereas the HXR spectra are dominated by components below approximately 80 MHz. This difference indicates that the energetic-electron response measured through HXR emission is not uniformly distributed among the fluctuation modes observed by the magnetic diagnostics.

Comparisons between the forward- and backward-viewing configurations (Fig. 6(a)) and between the forward- and vertical-viewing configurations (Fig. 6(b)) reveal noticeable differences in the relative amplitudes of several spectral components. In particular, substantial asymmetry is observed for several spectral peaks, as indicated by the downward arrows in Fig. 6, suggesting that the diagnostic is sensitive to the directional properties of energetic-electron fluctuations.

In contrast, the two detectors with nearly identical forward-viewing sightlines (Fig. 6(c)) exhibit very similar spectral shapes, indicating that the differences observed in Figs. 6(a) and (b) are not primarily attributable to detector characteristics. These results demonstrate the capability of the diagnostic to detect high-frequency HXR

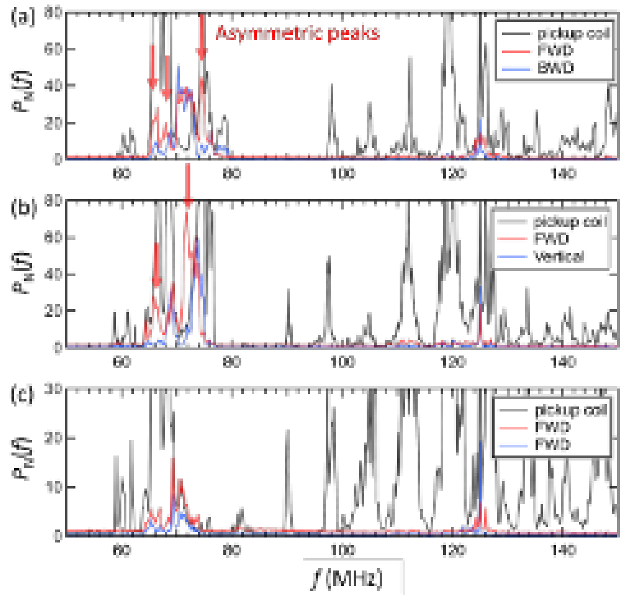

FIG. 6. Normalized fluctuation spectra, $P_{\rm N}(f)$, for different viewing configurations: (a) FWD–BWD (#57068), (b) FWD–Vertical (#57074), and (c) FWD–FWD (#57076). The red and blue curves denote the FHX2 and FHX1 detectors, while the black curve shows the simultaneously measured magnetic fluctuation spectrum. Downward arrows indicate frequencies at which substantial spectral asymmetry is observed between the two detector signals.

fluctuations and to resolve viewing-geometry-dependent features of energetic-electron dynamics.

IV. SUMMARY

A fast directional HXR diagnostic system based on plastic scintillators and PMTs has been developed for QUEST. During intense HXR emission, the detector response transitioned from pulse-counting to current-mode operation, enabling observation of high-frequency fluctuations in the HXR signal. Measurements using multiple viewing geometries revealed correspondence between magnetic and HXR fluctuations below approximately 80 MHz, together with directional differences in the HXR spectra. These results demonstrate the feasibility of high-frequency HXR fluctuation measurements as a new diagnostic of energetic-electron dynamics. The technique provides a unique experimental window into the dynamics of energetic-electron populations and their interaction with plasma waves, opening new opportunities for experimental studies of wave–particle interactions.

ACKNOWLEDGMENTS

The authors would like to thank all members of the QUEST experimental team for their support and assistance throughout this work.

This work was partly supported by JSPS KAKENHI (21K03511, 24K00606) and partly by NIFS collaboration research program (NIFS22KUTR172, NIFS25KFFT005).

[1] D.A. Spong *et al.*, Phys. Rev. Lett. **120**, 155002 (2018).
[2] W.W. Heidbrink *et al.*, Plasma Phys. Control. Fusion **61**, 014007 (2018).
[3] A. Lvovskiy *et al.*, Nucl. Fusion **59**, 124004 (2019).
[4] C. Liu *et al.*, Phys. Rev. Lett. **120**, 265001 (2018).
[5] C. Paz-Soldan *et al.*, Nucl. Fusion **59**, 066025 (2019).
[6] T.K. Cloarec *et al.*, Plasma Fusion Res. **21**, 1202010 (2026).
[7] R. Ikezoe *et al.*, Proc. of the 29th IAEA-FEC, (Queen Elizabeth II Centre, London 2023).
[8] N. Breizman *et al.*, Nucl. Fusion **68** 083001 (2019).
[9] S. Ratynskaia *et al.*, Plasma Phys. Control. Fusion **59** 053501 (2026).
[10] A.N. James, E.M. Hollmann, G.R. Tynan, Rev. Sci. Instrum. **81**, 10E306 (2010).
[11] A. Dal Molin *et al.*, Rev. Sci. Instrum. **92**, 043517 (2021).
[12] A.E. Shevelev *et al.*, Nucl. Instrum. Methods Phys. Res. A **830**, 102 (2016).
[13] D.C. Pace *et al.*, Rev. Sci. Instrum. **87**, 043507 (2016).
[14] C. Paz-Soldan *et al.*, Phys. Plasmas **25**, 056105 (2018).
[15] R.J. Zhou, Phys. Rev. E **107**, 045204 (2023).
[16] S. Guan *et al.* JINST **21** P06041 (2026).
[17] T. Barbui *et al.* Rev. Sci. Instrum. **95**, 083539 (2024).
[18] K. Hanada *et al.*, Plasma Fusion Res. **5**, S1007 (2010).
[19] K Hanada *et al.*, Plasma Phys. Control. Fusion 67, 115031 (2025).
[20] H. Idei *et al.*, Nucl. Fusion **57**, 126045 (2017).
[21] T. Onchi et al., Phys. Plasmas **28**, 022505 (2021).